CCC Annual Report

UIUC, August 20, 2014

Two-phase turbulent flow in a wide CC mold

Hyunjin Yang (ME PhD student)

Department of Mechanical Science & Engineering
University of Illinois at Urbana-Champaign

Research objectives

1. Simulate phenomena on the top surface in casting mold accurately. (through validation with nailboard experiment data)
2. Understand effects of continuous casting operation variables on the surface phenomena (slag and bubble entrainment) by a steady state parametric study (K-ε model)
3. Capture transient surface phenomena through a transient simulation (SAS model)

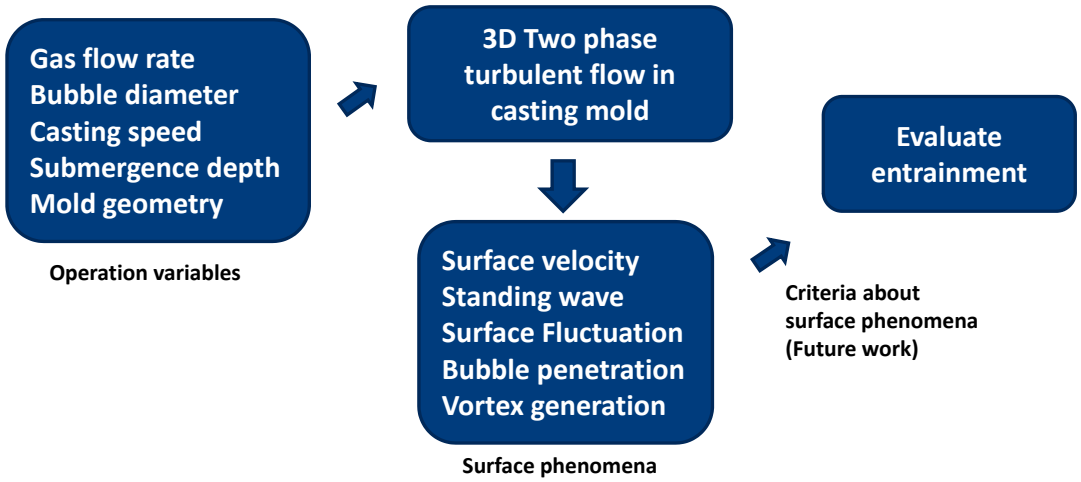

Computational domain

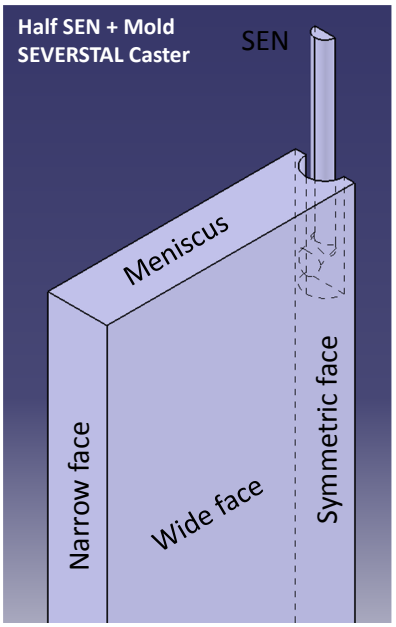

Fig 3. Computational geometry of the standard case by CATIA

- Liquid steel region is defined as a computational domain.

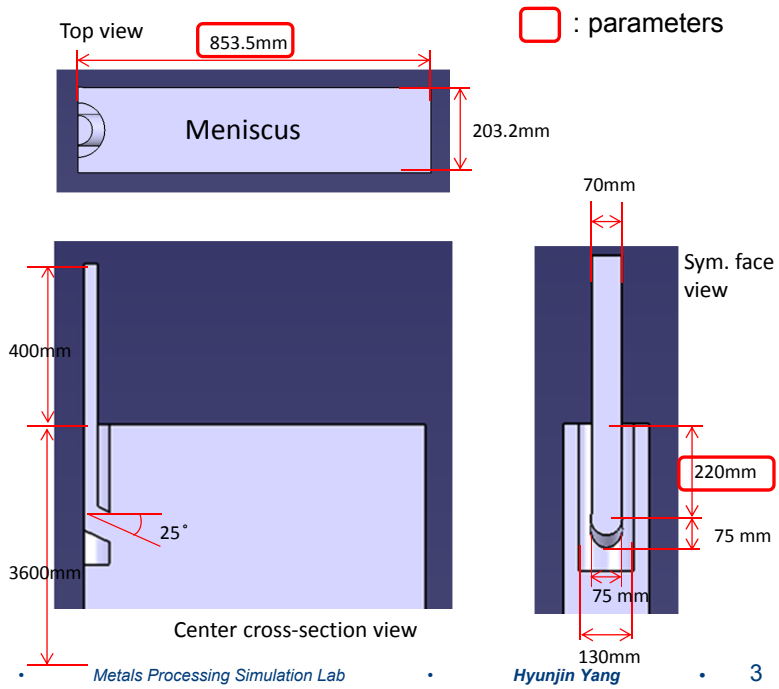

Mesh generation

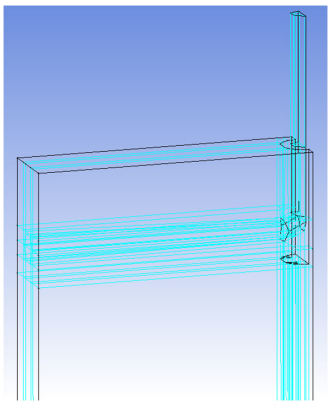

Fig 4. Block structure by ICEM-CFD

- Transfer the geometry from CATIA
- Split the domain using blocks
- generate a hexahedral mesh
- Cells: ~7mm cube
- Nodes : 1.3 million

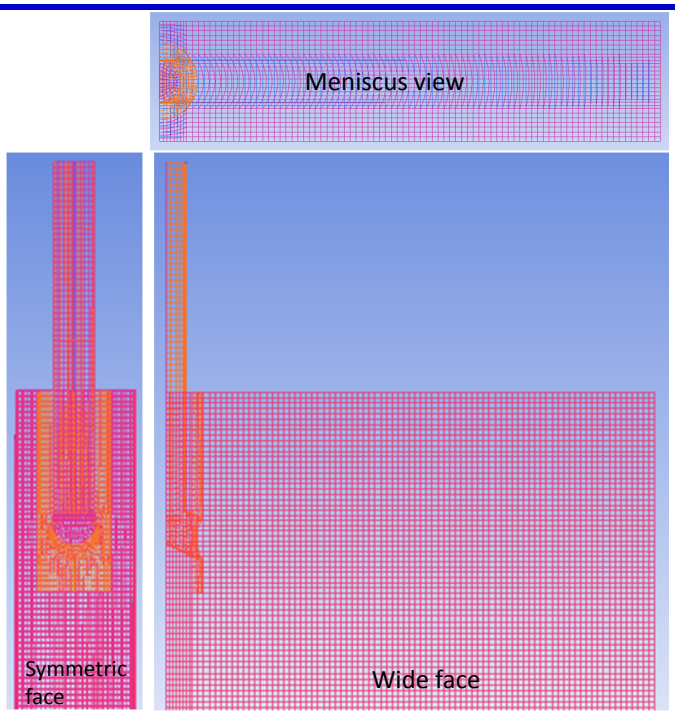

Fig 5. Mesh generation by ICEM-CFD

Boundary conditions

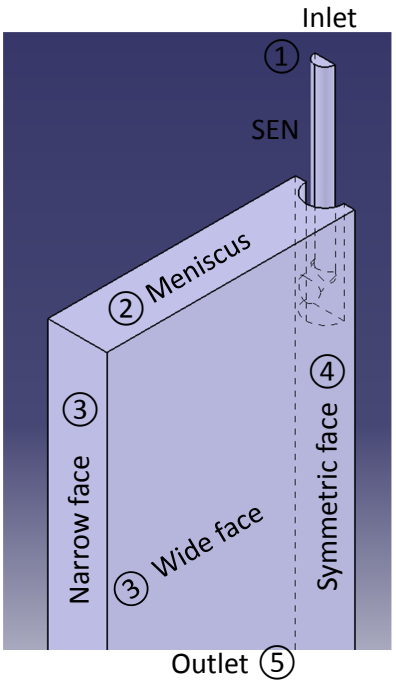

Fig 6. Schematic of the boundary conditions

① : constant velocity BC using the slide-gate UDF

② : free-slip BC with gas sink

③ : moving wall BC ($V_z = V_{casting}$)

④ : symmetric BC

⑤ : constant pressure BC

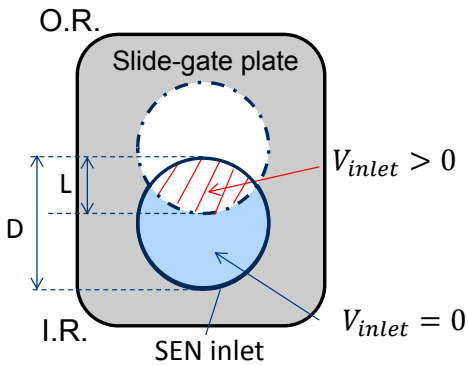

Fig 7. Schematic of the slide-gate BC using UDF

Slide gate opening fraction

$$F_L = \frac{L}{D}$$

$$F_A = \frac{A_{open}}{A_{SEN}}$$

Governing equations

3D Steady turbulent two phase flow simulation (K-ε + Eulerian model)

q : phase (liquid steel or Ar gas)
α : volume fraction
ρ : density
$\vec{u}$: velocity vector
p : pressure
$\vec{g}$: gravity acceleration
K_{pq} : momentum exchange coefficient
S_{ij} : strain rate tensor

$C_1 = 1.44$
$C_2 = 1.92$
$C_\mu = 0.09$
$\sigma_K = 1.0$
$\sigma_\varepsilon = 1.3$

1. Mass conservation

$$\nabla \cdot (\alpha_q \rho_q \vec{u}_q) = 0$$

2. Momentum conservation

$$\nabla \cdot (\alpha_q \rho_q \vec{u}_q \vec{u}_q) = \alpha_q \nabla p + \nabla \cdot ((\mu_q + \mu_{t,q}) \alpha_q \left(\nabla \vec{u}_q + \nabla \vec{u}_q{}^T\right)) + \alpha_q \rho_q \vec{g} + K_{pq}(\vec{u}_p - \vec{u}_q)$$

3. Turbulent kinetic energy K

$$\nabla \cdot (\rho_q \alpha_q \vec{u}_q K_q) = \nabla \cdot \left(\alpha_q (\mu_q + \frac{\mu_{t,q}}{\sigma_{K,q}}) \nabla K_q\right) - \alpha_q \rho_q \varepsilon_q + \alpha_q \mu_{t,q} S^2$$

4. Turbulence dissipation ε

$$\nabla \cdot (\rho_q \alpha_q \vec{u}_q \varepsilon_q) = \nabla \cdot \left(\alpha_q \left(\mu_q + \frac{\mu_t}{\sigma_{\varepsilon,q}} \nabla \varepsilon_q\right)\right) + \alpha_q C_1 \frac{\varepsilon_q}{K_q} \mu_{t,q} S^2 - \alpha_q C_2 \rho_q \frac{\varepsilon_q{}^2}{K_q}$$

$$\mu_{t,q} = C_\mu \rho_q \frac{K_q{}^2}{\varepsilon_q} \qquad S^2 = 2 S_{ij} S_{ij}$$

Process parameters: Standard condition(Nailboard 1)

Parameters	Values
Mold width	1707.0 mm
Slide-gate orientation	90.0 deg (toward Outer Radius)
Slide-gate opening fraction (f_L, f_A)	f_L=0.521 (f_A=0.415)
SEN submergence depth	220 mm
Liquid steel volume flow rate	0.0081 m^3/s
Casting speed	1.40 m/min (23.3 mm/s)
Argon gas volume fraction	5.8 %
Bubble diameter	5 mm

Material properties	Values
Viscosity of liquid steel	0.0067 Pas
Density of liquid steel	7000 kg/m^3
Viscosity of Ar gas	2.125e-05 Pas
Density of Ar gas	1.6228 kg/s

Single phase flow: Run1 (single phase)

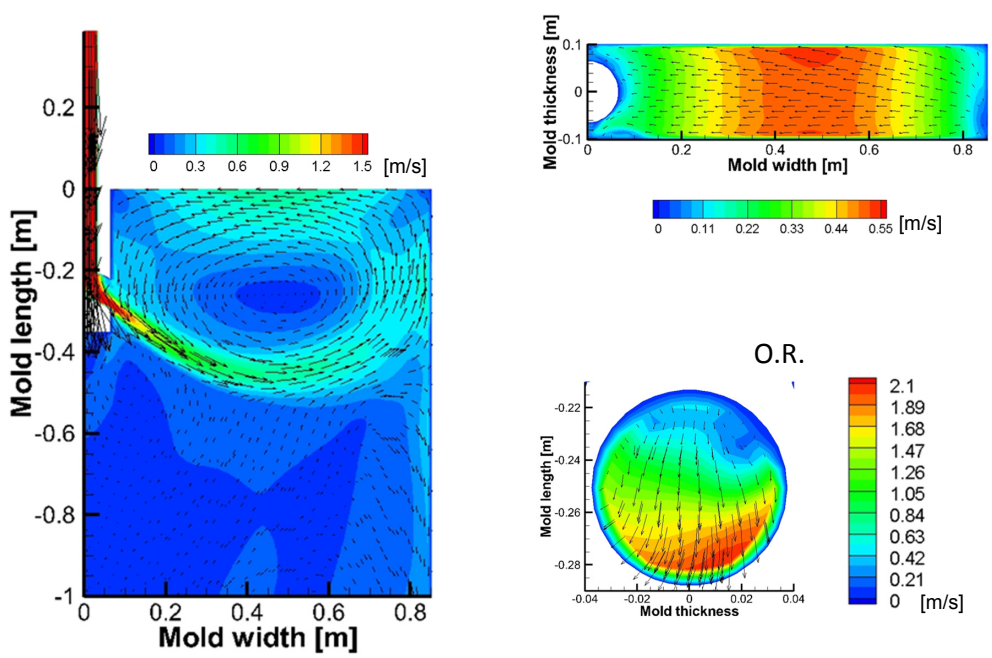

Fig. 8. molten steel velocity distribution on the center(left), meniscus(up) and port(right)

Two phase flow: Run2 (5mm bubble)

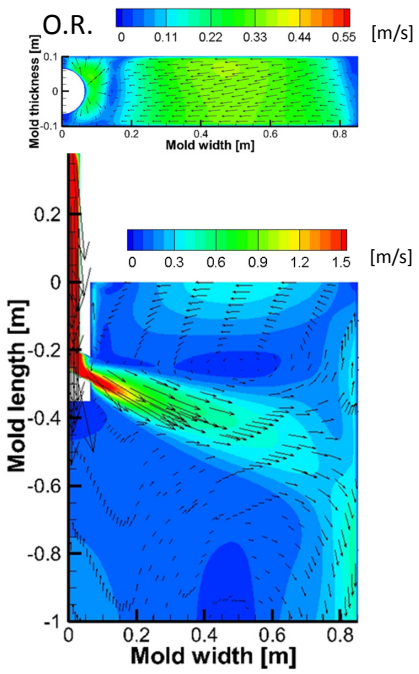

Fig. 9. molten steel velocity distribution on the center & meniscus

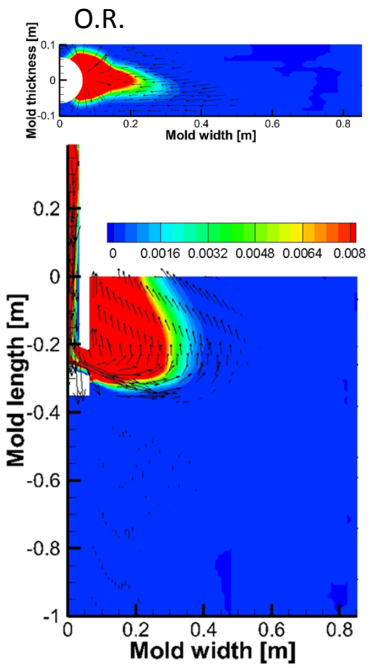

Fig. 10. Ar gas volume fraction distribution on the center & meniscus

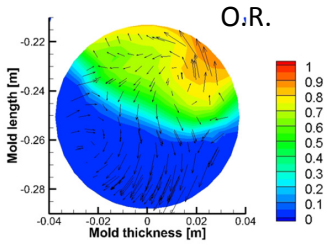

Fig. 11. Ar gas volume fraction and velocity vector on the port

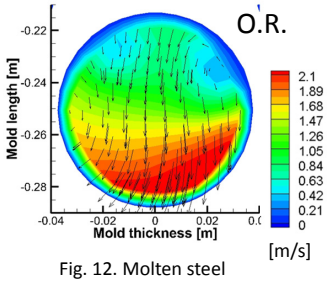

Fig. 12. Molten steel velocity on the port

Two phase flow: Run9 (3mm bubble)

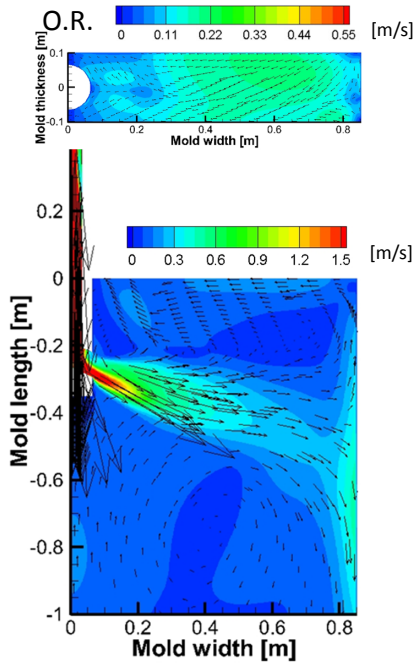

Fig. 13. molten steel velocity distribution on the center & meniscus

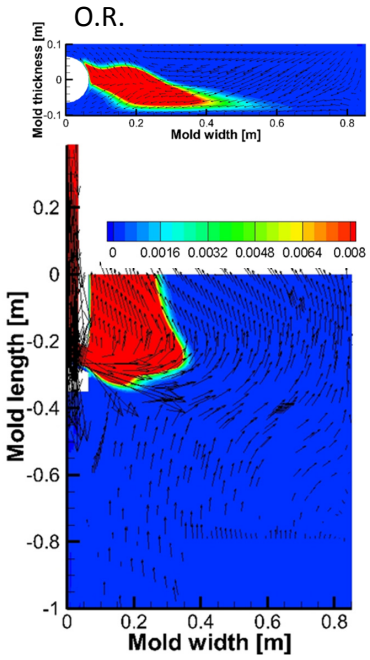

Fig. 14. Ar gas volume fraction distribution on the center & meniscus

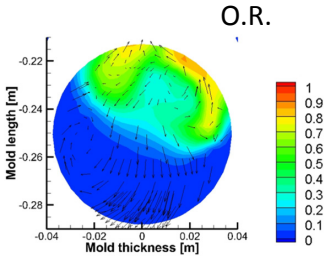

Fig. 15. Ar gas volume fraction and velocity vector on the port

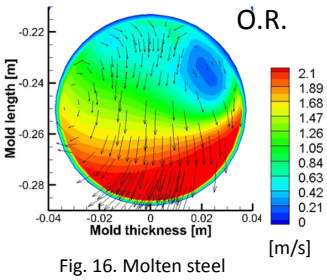

Fig. 16. Molten steel velocity on the port

Validation with experiment Run1, 2, 9 vs nailboard

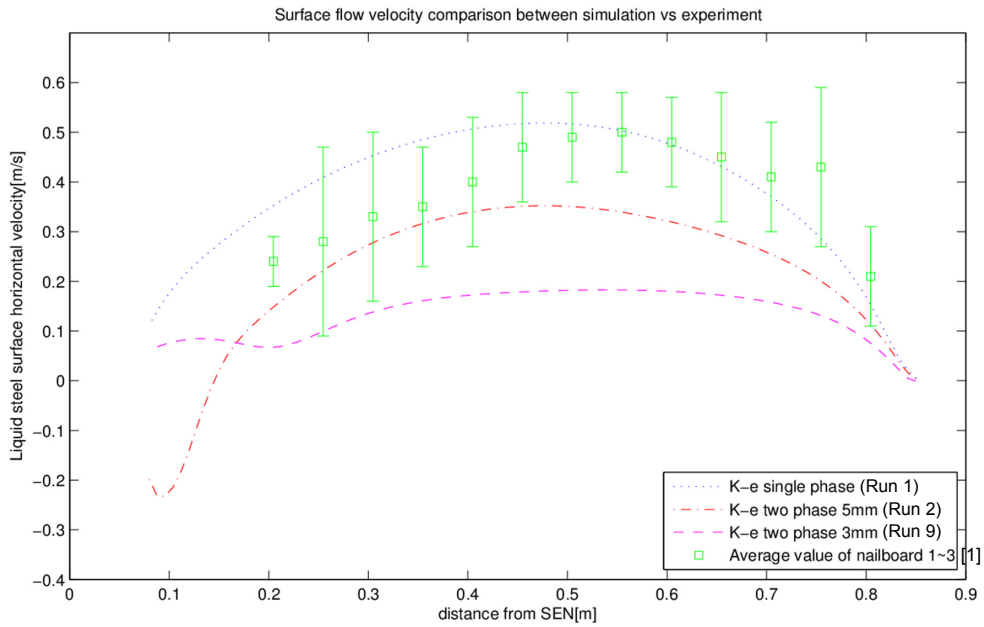

[1] nailboard data from CCC 2013 Chavan

Fig. 17. Liquid steel surface horizontal velocity comparison with the experiment

Validation with experiment Run1, 2, 9 vs nailboard

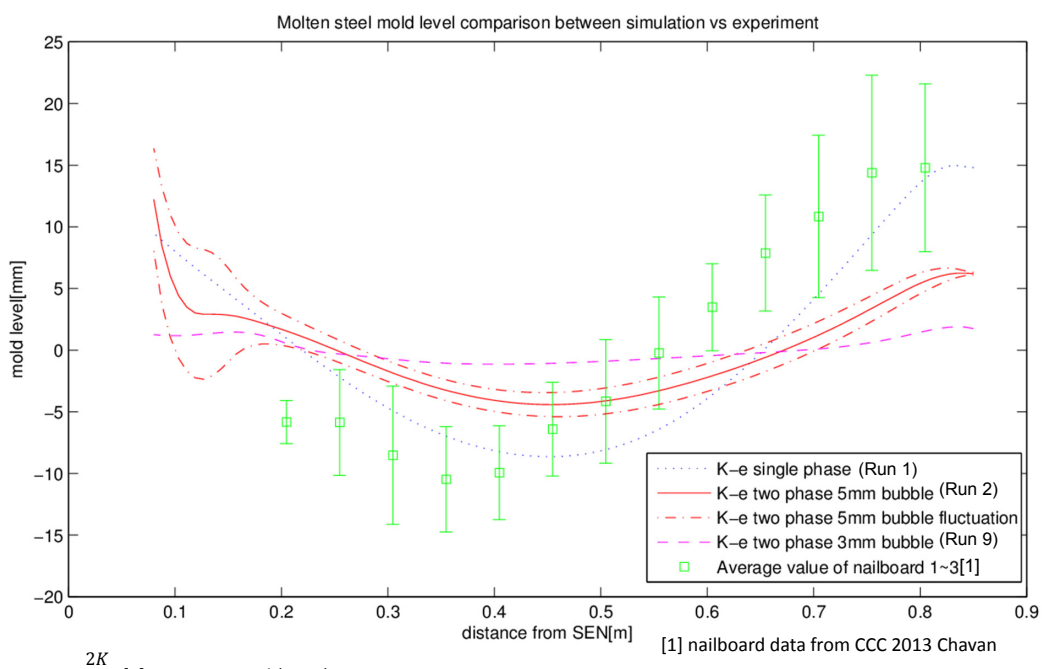

[1] nailboard data from CCC 2013 Chavan

$h_{fluctuation} = \frac{2K}{g}$ [2] X. Hwang et al.(1996)

Fig. 18. Mold level height comparison with the experiment

Conclusions: validation & single phase vs two phase (bubble size)

- Two phase flow simulation results show lower velocity magnitude and standing wave height than the nailboard experiment data & single phase flow simulation result.
- 5mm bubble result shows a better matching with the nailboard than the 3mm result.
  - 5mm bubble float immediately: generate a strong opposite flow near SEN
  - 3mm bubble is transported further & deeper: affect meniscus broadly and make the surface flow slow (but, no opposite flow)
- Large bubbles critically affect the bulk part of the flow pattern:
  - large bubble size is required to get a realistic flow pattern (regardless of the number of the bubbles)
  - Well educated bubble distribution is required for more accurate estimation.
- Steel flow exits the port towards the inner radius when the slide-gate is opened to the outer radius side: gas flow exits the outer radius side of the port towards the outer radius.
- These two flows together cause a cross flow on the top surface from outer radius to inner radius.

Parametric cases

	Gas volume fraction [%]	Slide-gate opening fraction	Mold width [mm]	Casting speed	Submergence depth [mm]	Bubble size [mm]	Tundish level [m]	Comparison
Run 1	0	f_L=0.521 (f_A=0.415)	1707	1.40 m/min (23.3 mm/s)	220	5	0.66	Volume fraction
Run 2	5.8	f_L=0.521 (f_A=0.415)	1707	1.40 m/min (23.3 mm/s)	220	5	0.87	Standard
Run 3	10	f_L=0.521 (f_A=0.415)	1707	1.40 m/min (23.3 mm/s)	220	5	0.98	Volume fraction
Run 4	5.8	f_L=0.425 (f_A=0.311)	1707	0.96 m/min (16.0 mm/s)	220	5	0.87	Slide-gate opening
Run 5	5.8	f_L=0.325 (f_A=0.211)	1707	0.64 m/min (10.7 mm/s)	220	5	0.87	Slide-gate opening
Run 6	5.8	f_L=0.521 (f_A=0.415)	1368	1.75 m/min (29.1 mm/s)	220	5	0.87	Mold width Casting speed
Run 7	5.8	f_L=0.521 (f_A=0.415)	1707	1.40 m/min (23.3 mm/s)	187	5	0.83	Submergence
Run 8	5.8	f_L=0.521 (f_A=0.415)	1707	1.40 m/min (23.3 mm/s)	160	5	0.80	Submergence
Run 9	5.8	f_L=0.521 (f_A=0.415)	1707	1.40 m/min (23.3 mm/s)	220	3	0.87	Bubble size
Run 10	5.8	f_L=0.450 (f_A=0.337)	1368	1.40 m/min (23.3 mm/s)	220	5	0.87	Mold width Slide-gate opening

Two phase flow: Run3 (α=10%)

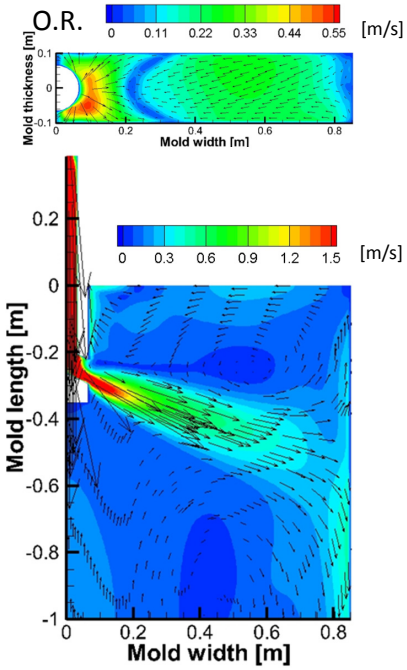

Fig. 19. molten steel velocity distribution on the center & meniscus

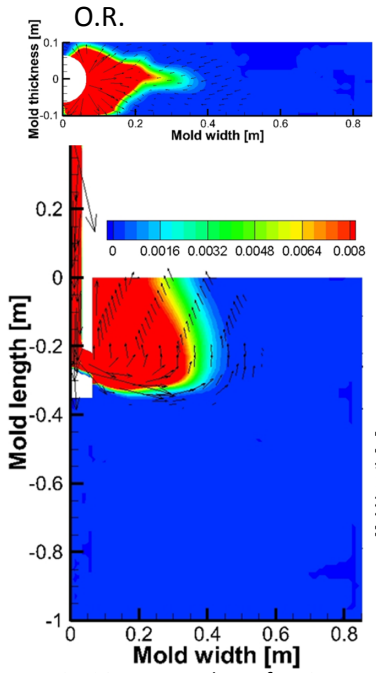

Fig. 20. Ar gas volume fraction distribution on the center & meniscus

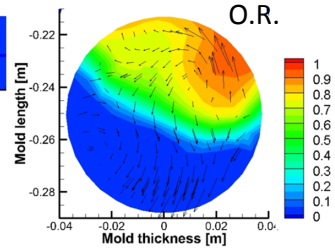

Fig. 21. Ar gas volume fraction and velocity vector on the port

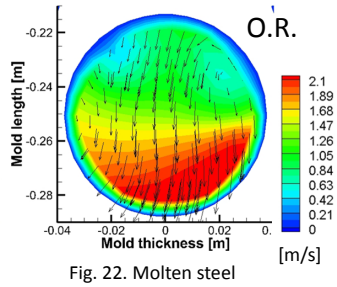

Fig. 22. Molten steel velocity on the port

Volume fraction effect on Surface velocity & Standing wave height

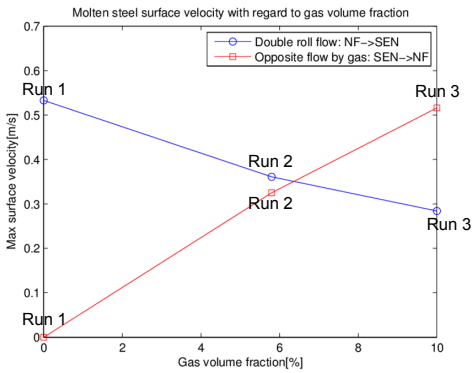

Fig. 23. Maximum surface velocity with regard to the gas volume fraction

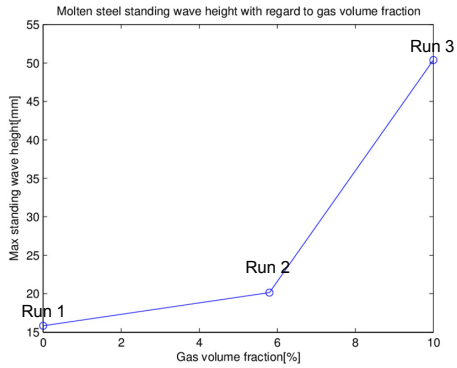

Fig. 24. Maximum standing wave height with regard to the gas volume fraction

- Increase of gas volume fraction strengthens the opposite flow and push back the double roll flow: two flows collide near SEN on the surface
- High gas volume fraction impinges top surface and cause a high standing wave near SEN.

Two phase flow: Run4 (f_L=0.425, $V_{casting}$=16.0mm/s)

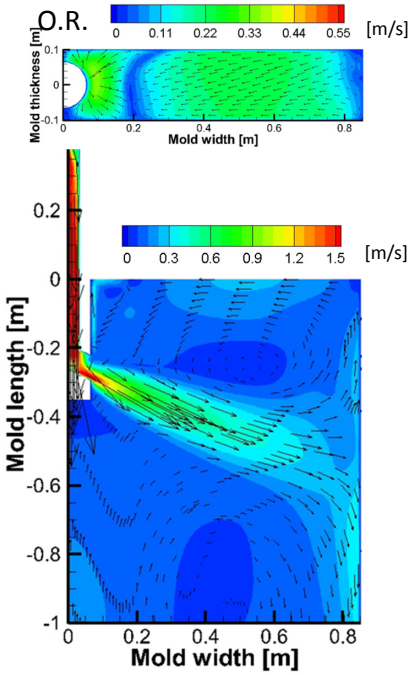

Fig. 25. molten steel velocity distribution on the center & meniscus

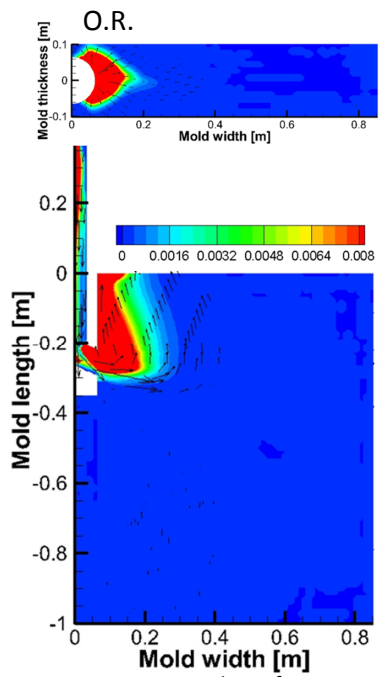

Fig. 26. Ar gas volume fraction distribution on the center & meniscus

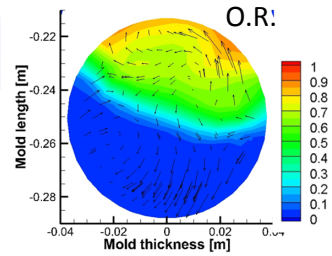

Fig. 27. Ar gas volume fraction and velocity vector on the port

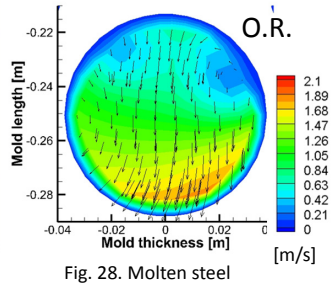

Fig. 28. Molten steel velocity on the port

Two phase flow: Run5 (f_L=0.325, $V_{casting}$=10.7mm/s)

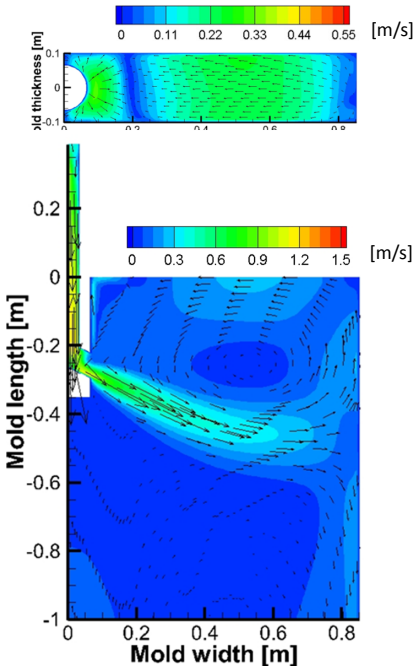

Fig. 29. molten steel velocity distribution on the center & meniscus

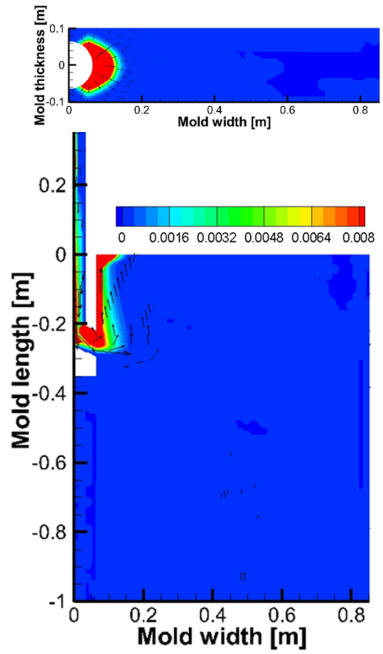

Fig. 30. Ar gas volume fraction distribution on the center & meniscus

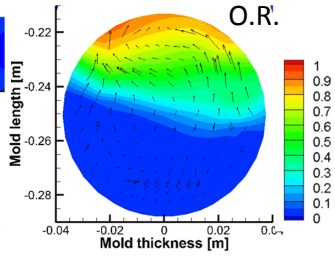

Fig. 31. Ar gas volume fraction and velocity vector on the port

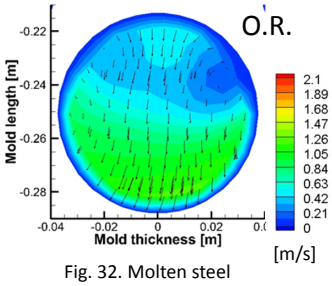

Fig. 32. Molten steel velocity on the port

Slide-gate effect on Surface velocity & Standing wave height

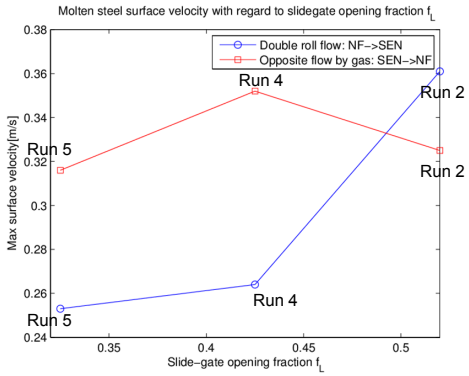

Fig. 33. Maximum surface velocity with regard to the gas volume fraction

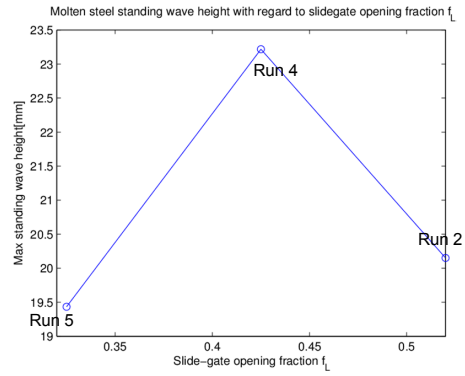

Fig. 34. Maximum standing wave height with regard to the gas volume fraction

- Increase of slide-gate opening fraction generates a higher flow rate for both fluids: cause a higher surface velocity for both flow.
- Fast liquid steel jet transport gas further from SEN : relieve the gas effect on the surface velocity and standing wave height (when f_L=0.52).

Two phase flow: Run7 (Sub. Depth=160mm)

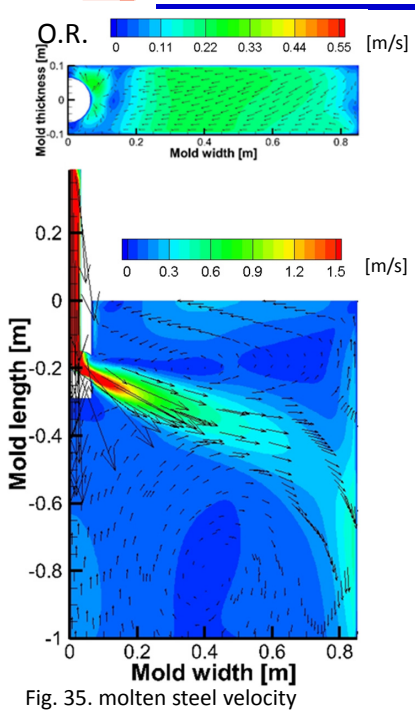

Fig. 35. molten steel velocity distribution on the center & meniscus

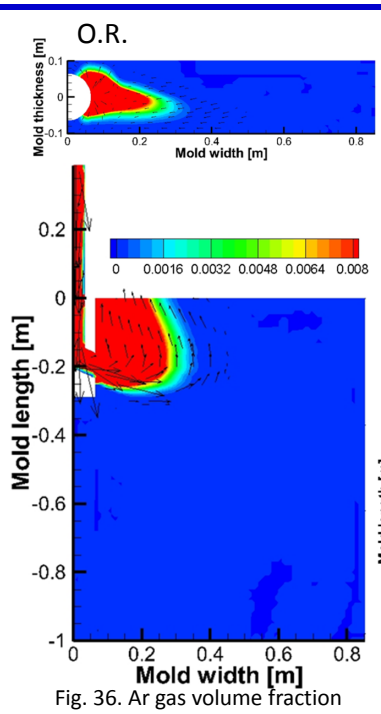

Fig. 36. Ar gas volume fraction distribution on the center & meniscus

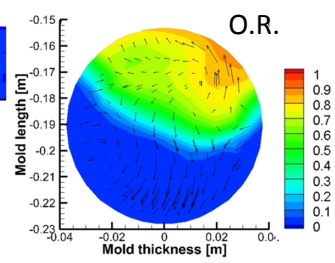

Fig. 37. Ar gas volume fraction and velocity vector on the port

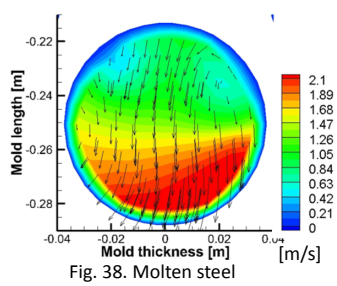

Fig. 38. Molten steel velocity on the port

Two phase flow: Run8 (Sub. Depth=187mm)

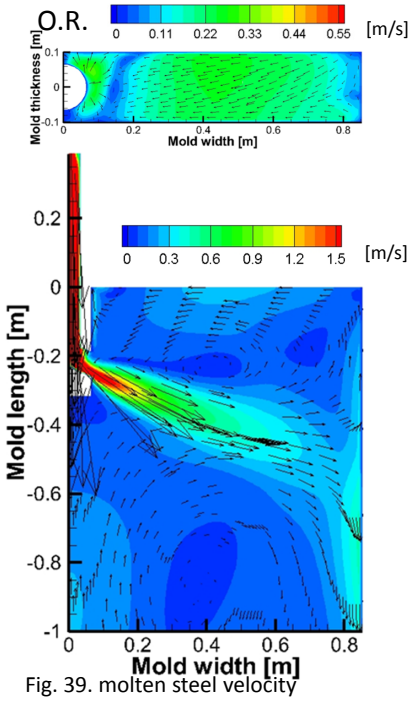

Fig. 39. molten steel velocity distribution on the center & meniscus

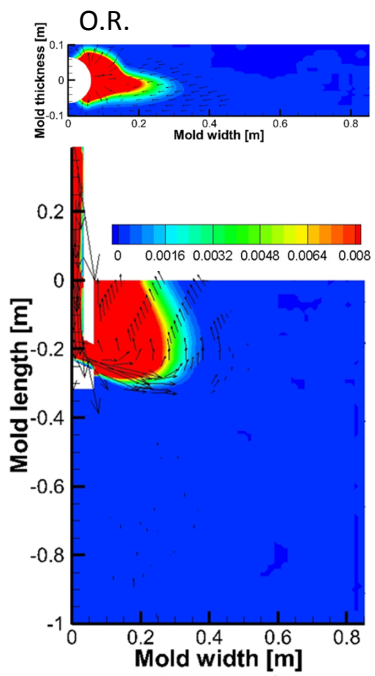

Fig. 40. Ar gas volume fraction distribution on the center & meniscus

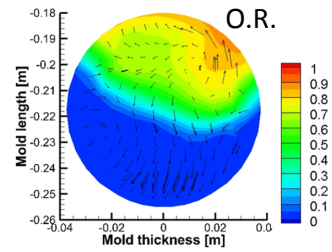

Fig. 41. Ar gas volume fraction and velocity vector on the port

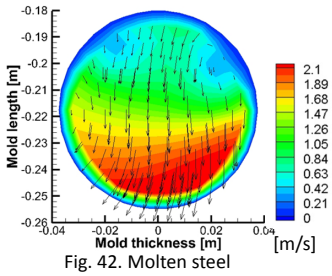

Fig. 42. Molten steel velocity on the port

Submergence depth effect on Surface velocity & Standing wave height

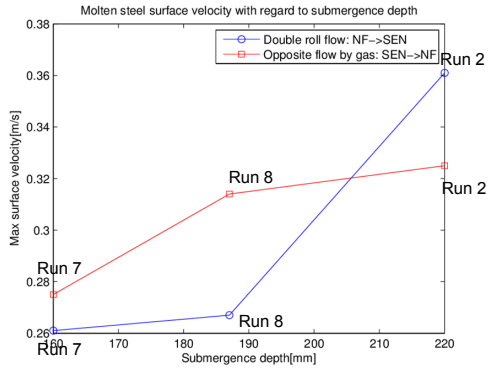

Fig. 43. Maximum surface velocity with regard to the gas volume fraction

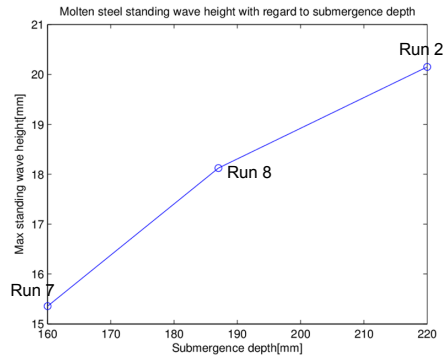

Fig. 44. Maximum standing wave height with regard to the gas volume fraction

- Deeper submergence depth increases both flow velocity magnitude.
  - Jet and double roll surface flow interact each other: both flow become slow by momentum diffusion when submergence depth is shallow.
  - Argon gas gets more rising velocity in the deep submergence depth -> cause a stronger opposite flow

Surface Vx comparison
Submergence depth: 220mm, 187mm, 160mm

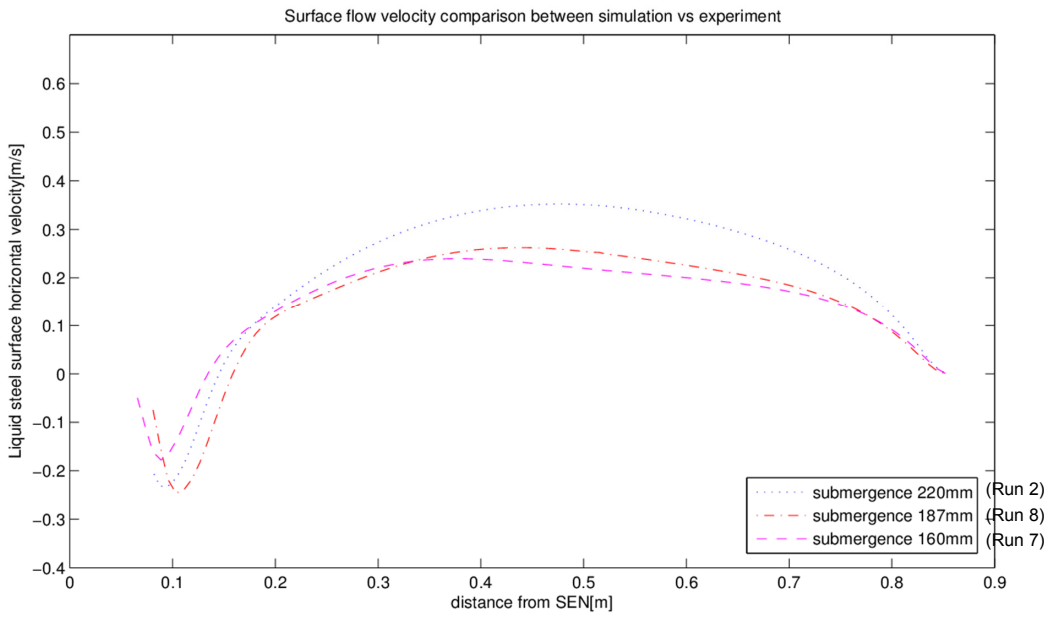

Fig. 44. Liquid steel surface horizontal velocity comparison with the experiment

Standing wave height comparison
submergence depth: 220mm, 187mm, 160mm

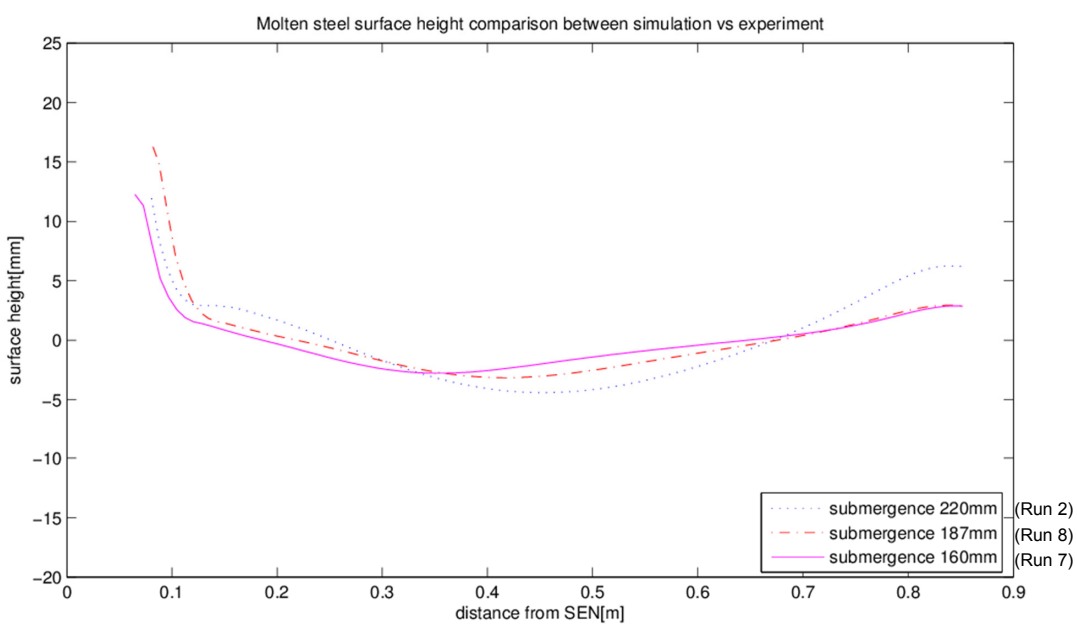

Fig. 44. Mold level height comparison with the experiment

Two phase flow: Run6
(mold width: 1368mm + Vc:1.75m/min)

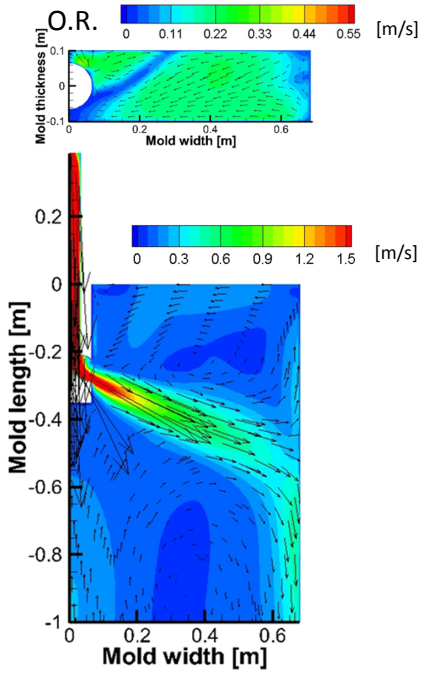

Fig. 45. molten steel velocity distribution on the center & meniscus

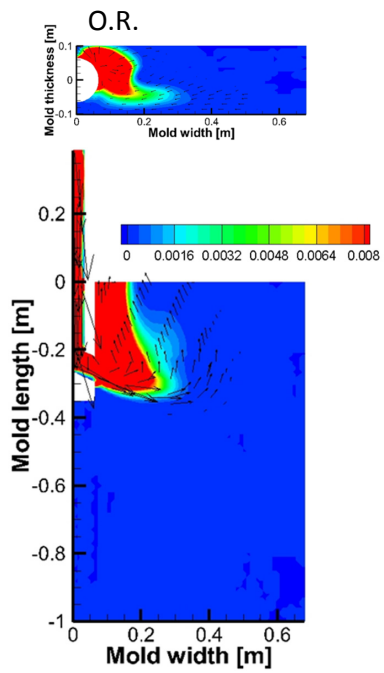

Fig. 46. Ar gas volume fraction distribution on the center & meniscus

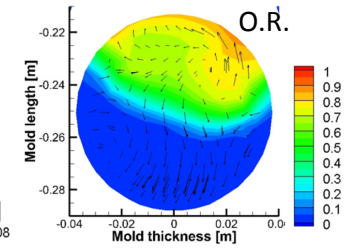

Fig. 47. Ar gas volume fraction and velocity vector on the port

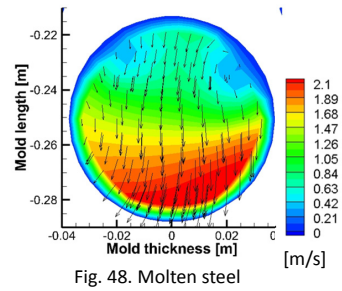

Fig. 48. Molten steel velocity on the port

Two phase flow: Run10
(mold width: 1368mm + Q_{steel}=0.0065m^3/s)

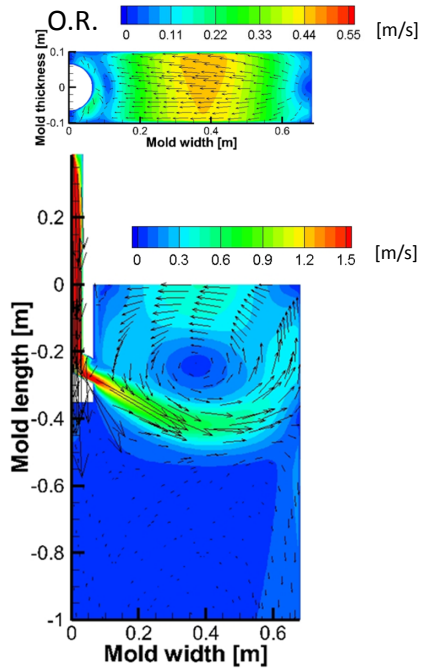

Fig. 49. molten steel velocity distribution on the center & meniscus

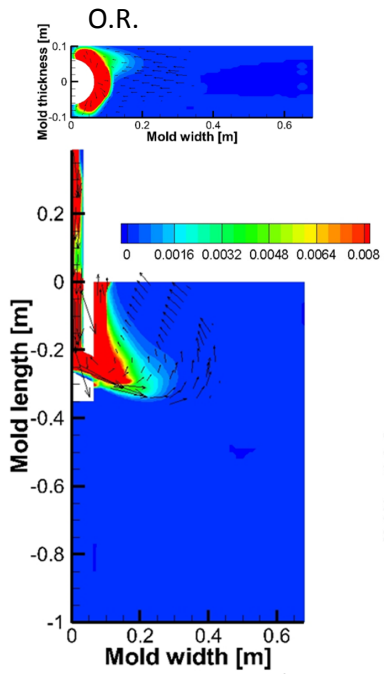

Fig. 50. Ar gas volume fraction distribution on the center & meniscus

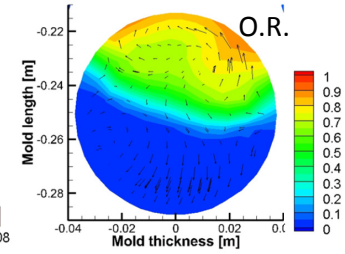

Fig. 51. Ar gas volume fraction and velocity vector on the port

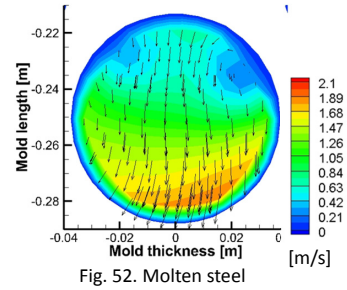

Fig. 52. Molten steel velocity on the port

Mold width effect on Surface velocity & Standing wave height

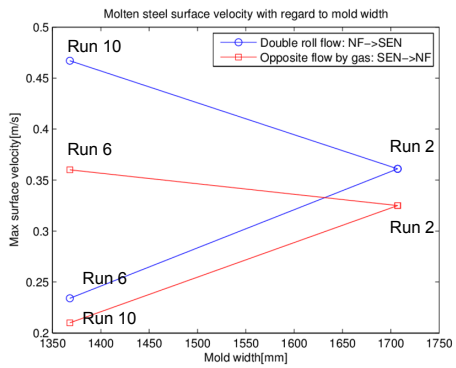

Fig. 53. Maximum surface velocity with regard to the gas volume fraction

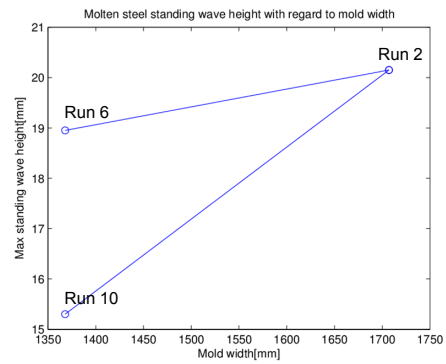

Fig. 54. Maximum standing wave height with regard to the gas volume fraction

- Run 6 (narrow mold width + constant steel flow rate) shows a stronger gas effect: higher opposite flow velocity by gas & lower double roll flow velocity than the standard condition (Run 2)
- Run 10 (narrow mold width + constant casting speed) shows a weaker gas effect: largest double roll flow velocity & lowest opposite flow velocity (like a single phase flow)

Parametric study result table

	Upper eye location at the center plane {x,z}(m)	Narrow face Impingement Point {y,z}(m)	Max. Surface Velocity (m/s) + : NF -> SEN - : SEN -> NF	Maximum standing wave height [mm]
Run 1	0.473,-0.264	-0.0979,-0.451	+0.533	15.84
Run 2	0.507,-0.248	-0.0866,-0.513	+0.361(-0.325)	20.15
Run 3	0.566,-0.247	-0.0865,-0.525	-0.516(+0.284)	50.38
Run 4	0.531, -0.248	-0.0822,-0.520	-0.352(+0.264)	23.22
Run 5	0.527, -0.251	-0.0583,-0.465	-0.316(+0.253)	19.43
Run 6	0.361,-0.223	-0.073,-0.504	-0.360(+0.234)	18.95
Run 7	0.367,-0.200	-0.087, -0.464	-0.275(+0.261)	18.12
Run 8	0.132,-0.137	-0.097,-0.403	-0.314(+0.267)	15.36
Run 9	undefined	-0.0851,-0.471	+0.205	4.82
Run 10	0.369, -0.238	-0.004,-0.396	+0.467(-0.21)	15.3

Parametric study result table

	Maximum Surface K $[m^2/s^2]$	Maximum Surface fluctuation [mm]	Max. Gas Penetration [m]
Run 1	4.93e-3	1.56	-
Run 2	2.67e-2	8.47	-0.37
Run 3	5.16e-2	16.4	-0.375
Run 4	1.85e-2	5.87	-0.345
Run 5	1.53e-2	4.85	-0.31
Run 6	3.60e-2	11.4	-0.383
Run 7	2.44e-2	7.74	-0.309
Run 8	1.92e-2	6.09	-0.308
Run 9	2.22e-2	7.04	-0.375
Run 10	3.28e-2	10.4	-0.376

$$h_{fluctuation} = \frac{2K}{g}$$ [2] X. Hwang et al.(1996)

Practical Conclusions: Steady state parametric study

1. Upper eye location: shows a flow pattern (double roll flow pattern or transition).
2. Narrow face impingement point: jet is bent toward inner radius direction (-y). (by the outer radius slide-gate orientation)
3. Maximum surface velocity
   - Double roll flow(NF → SEN): velocity increases as bubble size↑, gas volume fraction↓, slide-gate opening fraction ↑, submergence depth ↑
   - Opposite flow(SEN → NF): velocity increases as bubble size↑, gas volume fraction ↑, submergence depth ↑
4. Maximum standing wave height
   - Increases as bubble size↑, gas volume fraction ↑, submergence depth ↑ and mold width ↑

Test a new transient turbulence model

Scale Adaptive Simulation

- Modified SST K-ω model : additional source tern Q_{SAS} in the Turbulence eddy frequency equation -> reduce the μ_t to LES level and capture unsteady phenomena.
- Relaxed mesh requirement & faster calculation speed than LES.

- Turbulent kinetic energy *K*

$$\frac{\partial \rho k}{\partial t} + \frac{\partial}{\partial x_i}(\rho u_i k) = \frac{\partial}{\partial x_j}\left[\left(\mu + \frac{\mu_t}{\sigma_k}\right)\frac{\partial k}{\partial x_j}\right] + \mu_t S^2 - \rho c_\mu k \omega$$

- Turbulence eddy frequency ω

Additional source term

$$\frac{\partial \rho \omega}{\partial t} + \frac{\partial}{\partial x_i}(\rho u_i \omega) = \frac{\partial}{\partial x_j}\left[\left(\mu + \frac{\mu_t}{\sigma_\omega}\right)\frac{\partial \omega}{\partial x_j}\right] + \alpha \frac{\omega}{k}\mu_t S^2 - \rho \beta \omega^2 + (1 - F_1)\frac{2\rho}{\sigma_{\omega,2}}\frac{1}{\omega}\frac{\partial k}{\partial x_j}\frac{\partial \omega}{\partial x_j} + \boxed{Q_{SAS}}$$

SAS single phase flow: Run 1 transient Animations

Mesh size: 1.8 million

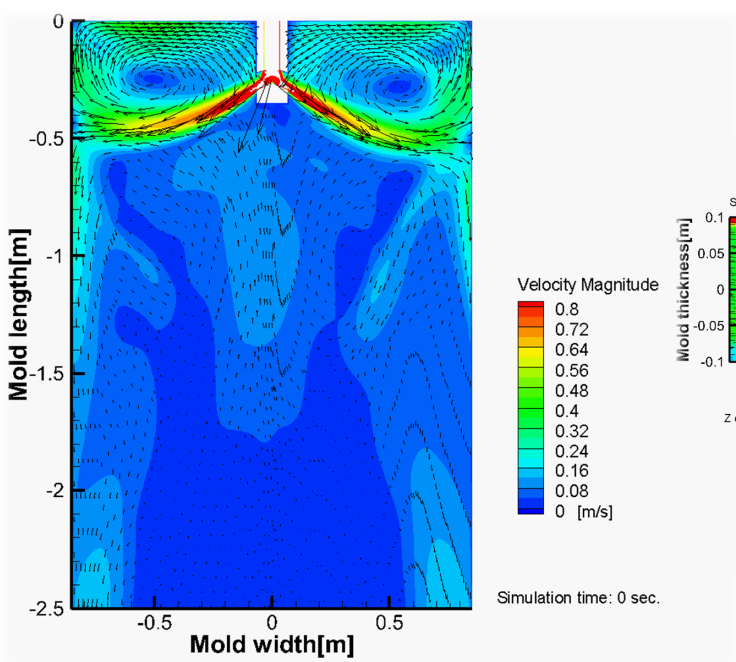

Center plane velocity distribution

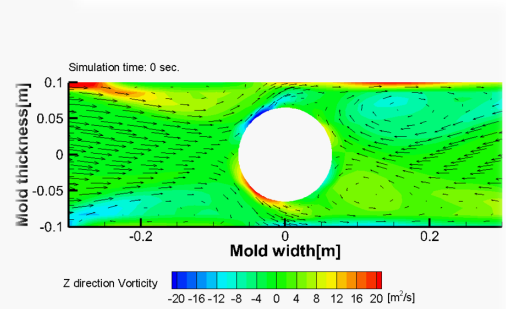

Top surface vortex shedding

Nailboard validation result

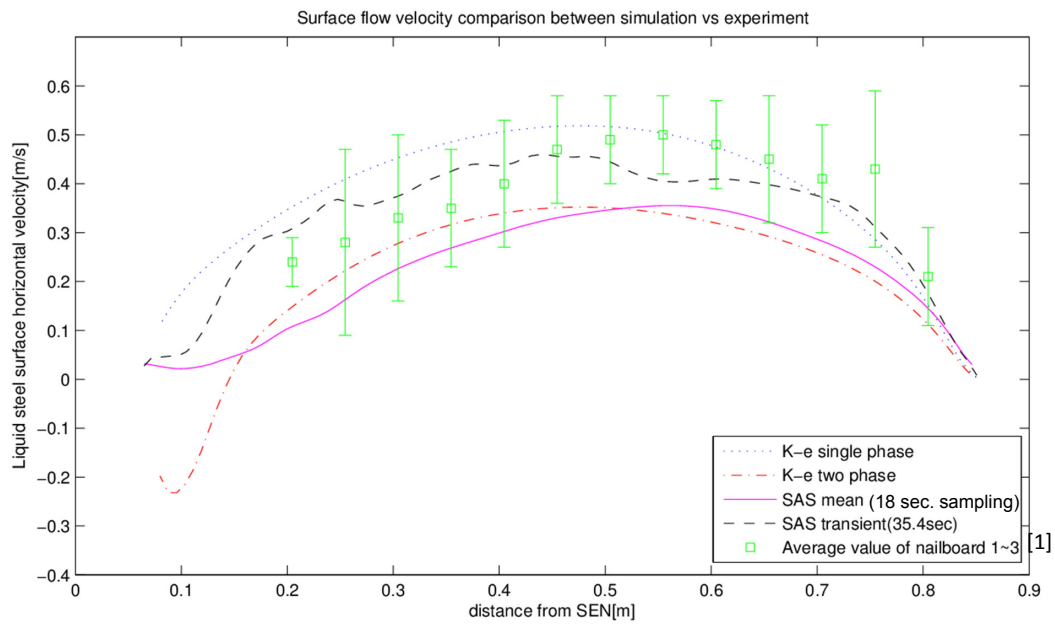

[1] nailboard data from CCC 2013 Chavan

Fig. 53. Liquid steel surface horizontal velocity comparison with the experiment

Nailboard validation result

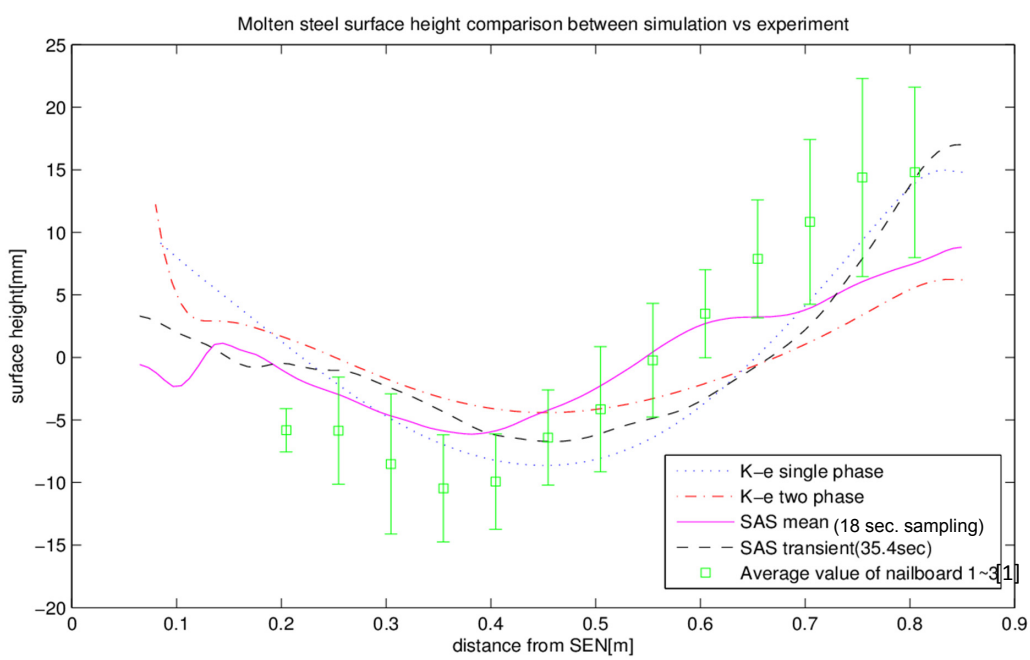

[1] nailboard data from CCC 2013 Chavan

Fig. 54. Mold level height comparison with the experiment

Conclusion & Future work: SAS single phase simulation

- SAS model can predict a transient surface phenomena
  : promising method to evaluate transient entrainment mechanisms
  (vortex generation near SEN top surface, surface height fluctuation etc.)

- SAS mean results (sampling time=18sec) roughly match to the nailboard data
  : SAS mean velocity shows a lower magnitude than the K-ε single phase steady result

- Faster calculation time with coarser mesh
  - 10 seconds calculation (time step=0.01 sec.) /day with 6-core (Xeon X5650) workstation
  - does not need any explicit requirement for a mesh design
  (such as a certain number of nodes are required inside of the boundary layer for LES, DES)

- Two phase flow simulation is available with DPM (future work).

Acknowledgments

- Continuous Casting Consortium Members (ABB, ArcelorMittal, Baosteel, Magnesita Refractories, Nippon Steel and Sumitomo Metal Corp., Nucor Steel, Postech/ Posco, Severstal, SSAB, Tata Steel, ANSYS/ Fluent)

References

1. R. Liu, et al., “Measurement of molten steel surface velocity with SVC and nail dipping during continuous casting process.”, *The Minerals, Metals & Materials Society,* 2011.
2. M. Chavan, “Nailboard measurements of surface flow at Severstal”, *CCC annual report* , 2013
3. Bai, H., et al., “Turbulent Flow of Liquid Steel and Argon Bubbles in Slide-Gate Tundish Nozzles, Part I, Effect of Operation Conditions and Nozzle Design,” *Metallurgical and Materials Transactions B*, 32B:2, 269-284, 2001.
4. Bai, H., et al., “Turbulent Flow of Liquid Steel and Argon Bubbles in Slide-Gate Tundish Nozzles, Part II, Effect of Operation Conditions and Nozzle Design,” *Metallurgical and Materials Transactions B*, 32B:2, 269-284, 2001.
5. R. Singh, B.G. Thomas and S.P. Vanka, “Large eddy simulations of double-ruler electromagnetic field effect on transient flow during continuous casting.”, *Metallurgical and Materials Transactions B*, 2014
6. Levy, S., “Two phase flow in complex systems”, 1999
7. White, F., “Fluid dynamics”, 2013
8. D. Creech, “Computational modeling of multiphase turbulent fluid flow and heat transfer in the continuous slab casting mold,” Master thesis, 1999.
9. Hibbeler, L.C., et al., “Mold Slag Entrainment Mechanisms in Continuous Casting Molds.”, *Iron and Steel Technology*, 10:10, 121-136, Oct., 2013.
10. F.R. Menter et al., “A scale-Adaptive simulation model using two-equation models”, 43rd AIAA Aerospace sciences meeting and exhibit 10-13 January 2005, Reno, Nevada
11. Ansys, Inc, ANSYS FLUENT theory manual
12. X. Huang and B.G. Thomas, "Modeling Transient Flow Phenomena in Continuous Casting of Steel," in 35th Conference of Metallurgists , 23B, C. Twigge-Molecey, eds., (Montreal, Canada: CIM, 1996), 339-356.